Inelastic Scattering Cross Sections for 200- and 400-keV Electrons

C. E. Dick and J. W. Motz
National Bureau of Standards, Washington, D. C. 20234
(Received 9 January 1968)

With 200- and 400-keV electrons incident on thin targets of aluminum, copper, tin, and gold, experimental data are given for the pulse-height distributions produced in a silicon detector by the electrons scattered at angles of 40°, 90°, 120°, and 140°. These distributions were analyzed to determine the inelastic cross sections integrated over the energies of the scattered electrons in the energy region below the elastic peak. This lower energy region involves energy transfers that are large compared to the atomic binding energies, and most probably involves atomic ionization processes. The results show that these inelastic scattering cross sections increase sharply for angles larger than 90°, so that the ratio of the inelastic to the elastic cross sections becomes larger than unity. In addition, these large-angle inelastic cross sections increase with the atomic number of the target and with the average binding energy per target electron. Because of the unavailability of accurate calculations for this process, comparisons are made with the Møller cross sections for electron-electron scattering in order to demonstrate how atomic binding effects influence large-angle inelastic scattering.

1. INTRODUCTION

THE dominant processes that contribute to the inelastic scattering of electrons by atoms depend on the initial electron energy. For electrons with initial kinetic energies in the region of the electron rest energy ($\approx$500 keV), which is intermediate between atomic and nuclear binding energies, inelastic scattering occurs primarily because of (a) bremsstrahlung emission and (b) atomic excitation and ionization effects.

The inelastic electron scattering that is produced by the bremsstrahlung process has been calculated in the first Born approximation by Racah,[1] McCormick, Keiffer, and Parzen,[2] and Maximon and Isabelle.[3] These calculations predict the energy spectrum of electrons scattered at a given angle from thin targets with a given atomic number. Although the Born approximation is not valid in this intermediate energy region, these calculations can be expected to give at least an order-of-magnitude estimate[4] of the inelastic scattering arising from bremsstrahlung effects.

The inelastic electron scattering that is produced by atomic excitation and ionization effects has been studied extensively in the nonrelativistic energy region. However, at the present time, there is no satisfactory theoretical treatment of this process that applies to this intermediate energy region and that can predict the energy or angular distributions of the scattered electrons. Among the pertinent studies on electron-atom inelastic scattering are the calculations of Morse[5] and Weber, Deck, and Mullin.[6] Morse's calculations give the scattering cross section for inelastic electron-atom collisions as a function of the momentum transfer and are valid only for small angles (less than approximately 10°), small energy losses (small compared to the electron rest energy), and nonrelativistic electron energies. On the other hand, the calculations of Weber, Deck, and Mullin give the K-ionization cross-section differential with respect to the energy and angle of the scattered electrons, and are only valid for large scattering angles and for initial electron energies that are large compared to the electron rest energy. The inadequacy of the Weber, Deck, and Mullin calculations of inelastic energy spectra for intermediate electron energies has been previously revealed in comparisons with experimental data[7] on large-angle inelastic scattering of 500-keV electrons. Because of these limitations in the available calculations, it is necessary to rely on the Møller cross section[8] for approximate estimates of inelastic electron scattering at these intermediate energies, particularly for large energy losses and large scattering angles. The Møller cross section is limited by the fact that it applies only to electron scattering by free electrons, and therefore it gives predictions for inelastic scattering in the laboratory system, without the inclusion of binding effects, for scattering angles between 0° and 90°.

The present investigation provides additional data on large-angle inelastic scattering for electrons with initial kinetic energies of 200 and 400 keV. Data are obtained for the inelastic energy spectra of the electrons scattered by thin foils of aluminum, copper, tin, and gold at angles of 40°, 80°, 120°, and 140°. The inelastic cross sections that can be obtained from these data provide estimates of the contributions of atomic binding effects after the relative contribution of bremsstrahlung emission has been evaluated.

---

[1] G. Racah, Nuovo Cimento **11**, 476 (1934).
[2] P. T. McCormick, D. G. Keiffer, and G. Parzen, Phys. Rev. **103**, 29 (1956).
[3] L. C. Maximon and D. B. Iasbelle, Phys. Rev. **113**, B1344 (1964).
[4] Estimates of the accuracy of Born-type calculations are given by H. W. Koch and J. W. Motz, Rev. Mod. Phys. **31**, 920 (1959).
[5] P. M. Morse, Physik. Z. **33**, 443 (1932); see also, e.g., M. Pirenne, *Diffraction of X-rays and Electrons by Molecules* (Cambridge University Press, London, 1946), pp. 25, 54; U. Fano, Phys. Rev. **93**, 117 (1954); Gladys White Grodstein, Natl. Bur. Std. (U. S.), Circ. No. **583** (1957).
[6] T. A. Weber, R. T. Deck, and C. J. Mullin, Phys. Rev. **130**, 660 (1963); also G. W. Ford and C. J. Mullin, *ibid.* **110**, 520 (1958).
[7] J. W. Motz and R. C. Placious, Phys. Rev. **132**, 1120 (1963).
[8] C. Møller, Ann. Physik **14**, 568 (1932).

2. EXPERIMENTAL APPARATUS AND PROCEDURE

These measurements were carried out with the National Bureau of Standards 500-keV constant-potential accelerator. The accelerator electron beam was focussed to a 3-mm-diam spot on various targets located in the center of a 45-cm-diam scattering chamber which has provisions for detecting the scattered electrons at angles from 10° to 140° in 10° increments. The transmitted beam was collected in an aluminum Faraday cup and the total charge was measured with a current integrator with an accuracy of approximately 1%.

The scattered electron beam was detected by a surface barrier solid-state detector with a surface area of 25 mm² and a depletion depth of 500 μ. The detector pulses were amplified by a conventional amplifier system and the pulse-height distribution was measured with a multichannel analyzer. The scattered electrons entered the detector through an aluminum aperture system which subtended a solid angle of 9.5×10^{-5} sr with respect to the center of the target.

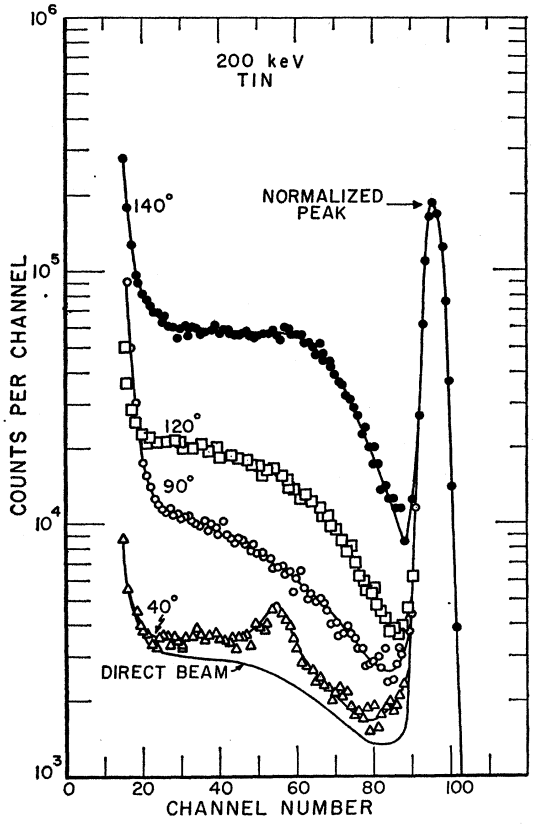

FIG. 1. Pulse-height distributions obtained by scattering 200-keV electrons from a thin target of tin into a silicon-detector spectrometer system at angles of 40°, 90°, 120°, and 140°. The direct-beam curve indicates the response of the detector to the unscattered electron beam. All curves are normalized to give the same value for the area under the elastic peak at the upper end of the distribution.

Because of the large variation of the elastic scattering cross section with scattering angle, the incident electron-beam direction was measured carefully at each energy by observing the position of the impinging beam on two phosphorescent screens, one located at the target position and one located approximately 45 cm above this position. With this procedure the scattering angle was determined with an accuracy of 0.5 mrad.

The pulse-height response of the solid-state detector to a monoenergetic electron beam was measured at 200 and 400 keV by placing the solid-state detector in the direct beam of the accelerator and reducing the current to a very low value ($\sim10^{-14}$–10^{-15} A). The energy spread of the accelerator beam is estimated to be less than ±100 eV. The line shapes obtained in these response curves were found to have a width of approximately 15 keV at half-maximum.

Measurements were made with incident beam currents of 3×10^{-9} and 6×10^{-9} A. At each incident energy of 200 and 400 keV, pulse-height distributions were measured at scattering angles of 40°, 90°, 120°, and 140°. The targets consisted of (a) self-supporting aluminum foils with thicknesses in the region from 25 to 160 μg/cm² and (b) evaporated foils of copper, tin, and gold with thicknesses in the region from 10 to 50 μg/cm² on

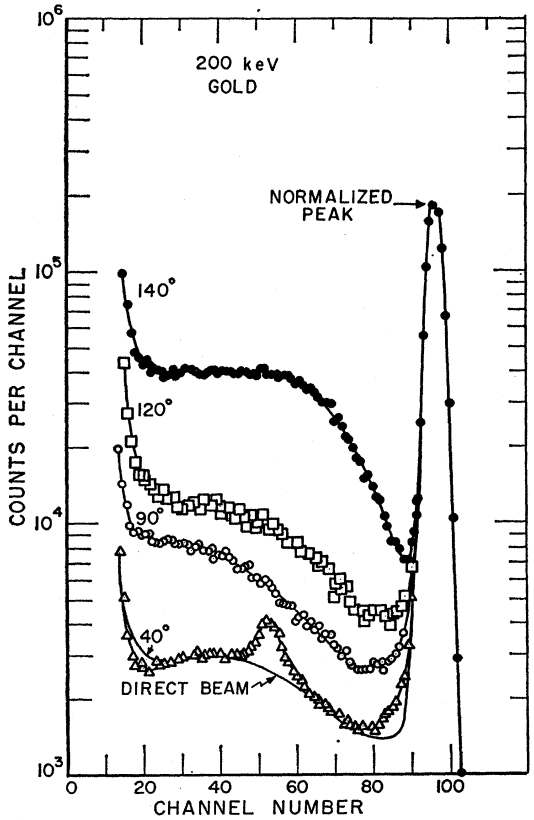

FIG. 2. Pulse-height distributions obtained by scattering 200-keV electrons from a thin target of gold. The other features are the same as in Fig. 1.

collodion backings with thicknesses in the region from 5 to 10 $\mu g/cm^2$. Pulse-height distributions for a given atomic number were obtained for two or more target thicknesses and these data indicated that the targets were thin enough so that multiple scattering effects were negligible.

3. RESULTS AND DISCUSSION

The experimental data are given by the pulse-height distributions in Figs. 1 and 2, respectively, for tin and gold at 200 keV, and in Figs. 3–6, respectively, for aluminum, copper, tin, and gold at 400 keV. The large peak at the upper end of each pulse-height distribution is produced mostly by the elastically scattered electrons (neglecting radiation effects) and the lower portion of the distribution is produced mostly by the inelastically scattered electrons. In each figure, the distributions for the different angles are normalized to give the same value for the area under the elastic peak. At 40°, the inelastic spectra show a small peak which is produced by electron-electron (Møller) scattering and at the remaining angles of 90°, 120°, and 140°, the inelastic spectra have a continuous distribution that is produced by the atomic binding effects in the scattering process. Also, the pulse-height response of the detector to the unscattered electron beam of 200 and 400-keV electrons is given by the direct-beam curve in which the low-energy tail is produced mostly by electrons back scattered from the detector. In all of these distributions, the channel number scale is linear with electron energy from zero to the incident electron energy which corresponds to the channel number at the elastic peak. The sharp rise below approximately 60 keV indicates the pulse-height region where the dominant contribution to the counts is produced by the noise in the detector system.

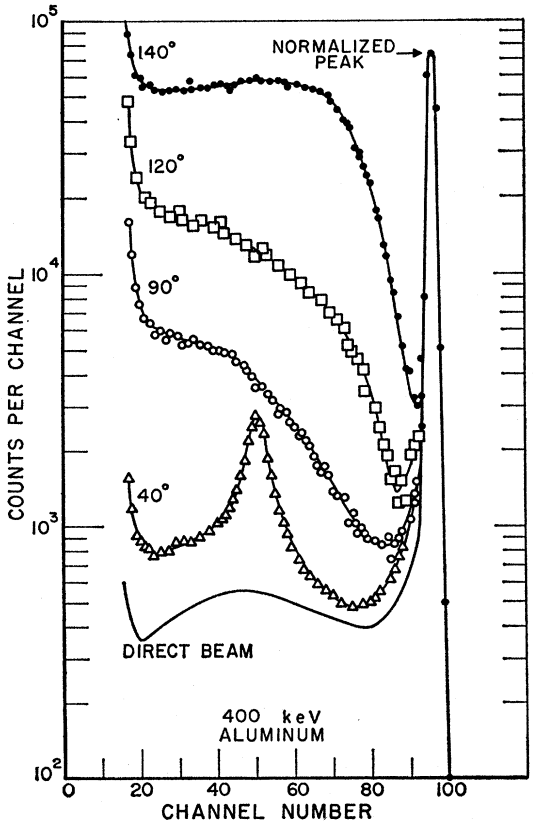

FIG. 3. Pulse-height distributions obtained by scattering 400-keV electrons from a thin target of aluminum. The other features are the same as in Fig. 1.

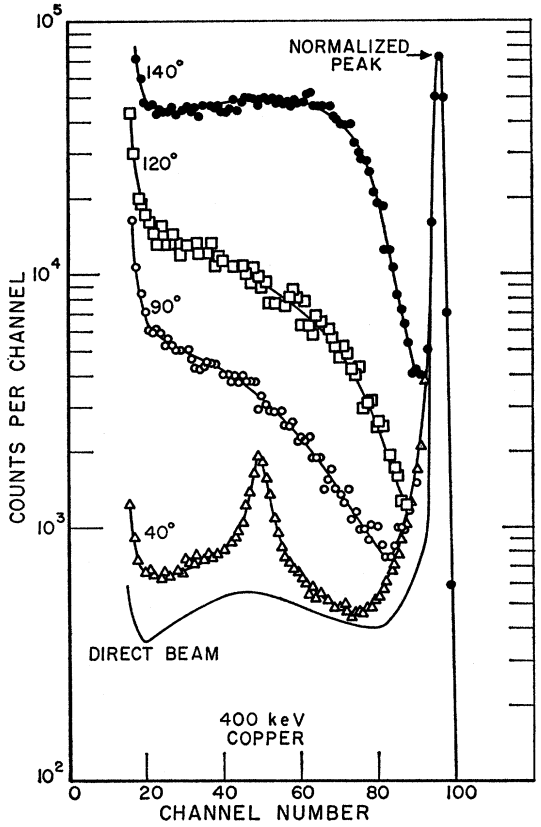

FIG. 4. Pulse-height distributions obtained by scattering 400-keV electrons from a thin target of copper. The other features are the same as in Fig. 1.

The elastic peaks which are shown in Figs. 1–6 include contributions from electrons that are inelastically scattered with energy losses in the region below approximately 10 keV. Also, these data show that there are no appreciable differences in the areas under the elastic peaks produced by the unscattered electrons (direct beam) and by the electrons scattered at the specified angles by a given target foil, and therefore, that most of the inelastic electrons contained in the elastic peak have suffered energy losses that are small compared to 10 keV. Such small energy losses most probably involve atomic excitation or soft-photon bremsstrahlung processes.

Below the elastic peak, the inelastic spectra show a rise in the counts with decreasing electron energies,

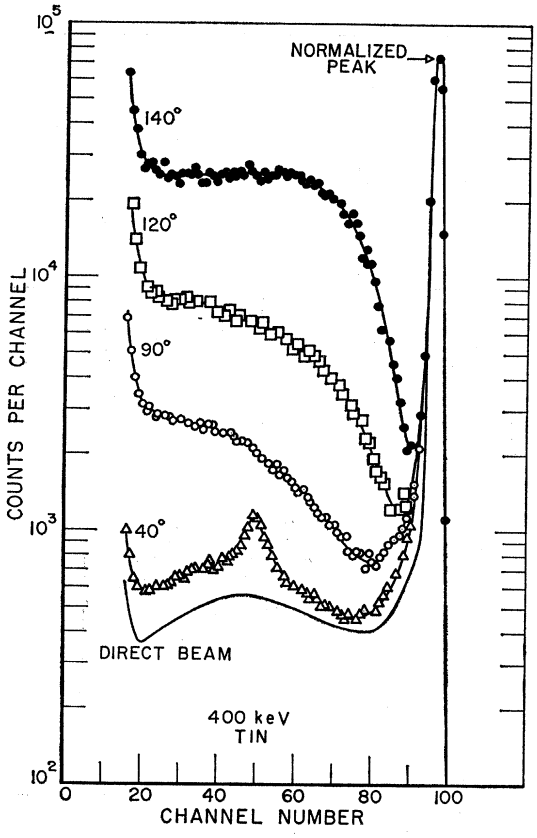

FIG. 5. Pulse-height distributions obtained by scattering 400-keV electrons from a thin target of tin. The other features are the same as in Fig. 1.

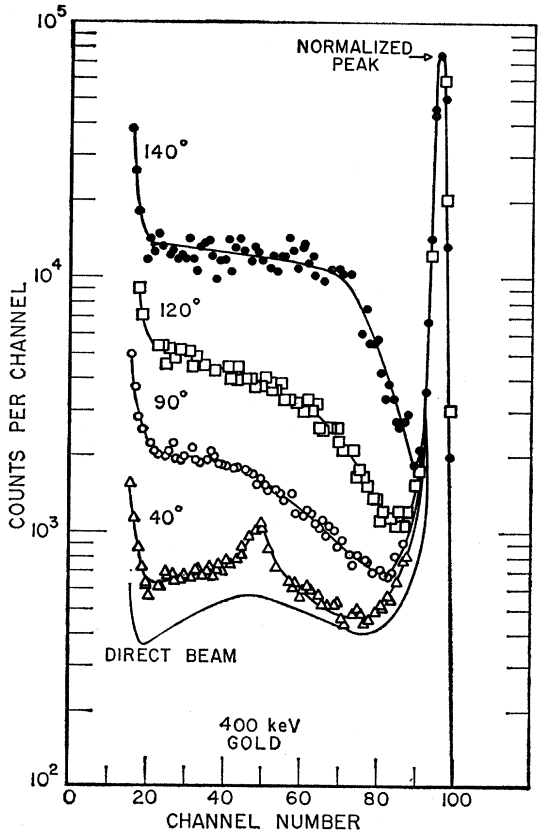

FIG. 6. Pulse-height distributions obtained by scattering 400-keV electrons from a thin target of gold. The other features are the same as in Fig. 1.

which is more rapid for the lower atomic numbers and larger angles. This behavior cannot be predicted[1–3,7] for electrons scattered in the bremsstrahlung process, for which the inelastic spectra show a decrease in the counts with decreasing electron energies and have negligible values compared to the measured spectra. Therefore the large energy transfers in this lower energy region most probably involve atomic ionization processes. However, in spite of the precautions taken, the possibility cannot be ruled out that there may still exist appreciable spurious scattering effects.

The pulse-height distributions in Figs. 1–6 may be used to evaluate inelastic ionization cross sections in the following manner. The number of counts $N(h)$ recorded by the spectrometer in a unit interval at the pulse height h after exposure to a given number $n(T_1)$ of scattered electrons per unit energy interval at the kinetic energy T_1 is given by

$$N(h)=R(h,T_1)n(T_1), \tag{1}$$

where the response function $R(h,T_1)$ gives the probability per incident electron that the spectrometer will record a count in a unit interval at the pulse height h. The integral $\int_0^{h_1} R(h,T_1)dh$ defines the spectrometer efficiency for the detection of electrons with energy T_1, where the upper pulse height limit h_1 is chosen so that $R(h,T_1)=0$ for $h\geq h_1$. In terms of this efficiency ϵ which is independent of the electron energy, Eq. (1) becomes

$$n(T_1)=\frac{1}{\epsilon}\int_0^{h_1} N(h)dh, \tag{2}$$

where $\int_0^{h_1} N(h)dh$ is the area under the pulse-height distribution. Therefore, for electrons that are elastically scattered with an energy T_1, the elastic cross section may be written as

$$\frac{d\sigma}{d\Omega}(\text{elastic})=\frac{n(T_1)}{mn_0\omega}=\frac{cA_{\text{DB}}}{mn_0\omega\epsilon}, \tag{3}$$

where m is the number of target atoms per cm^2, n_0 is the number of electrons incident on the target, ω is the solid angle subtended by the detector at a given scattering angle, c is a normalization constant, and A_{DB} is the area under the direct-beam curve in Figs. 1–6. The application of Eq. (3) to the present measurements requires that there is a negligible contribution to $n(T_1)$ from inelastically scattered electrons which have suffered small energy losses from other competing processes such as

atomic ionization, and which cannot be experimentally distinguished from the elastically scattered electrons. This condition has been verified in this energy and angular region by previous measurements,[9] in which good agreement has been obtained between exact theoretical elastic cross sections[10,11] and experimental cross sections derived from elastic peaks having an energy spread comparable to the peaks in Figs. 1–6. For electrons that are inelastically scattered in the energy region $0 \leq T \leq T_2$, where $T_2 = T_1 - \Delta T$ and ΔT is determined by the spectrometer energy resolution (15 keV in the present measurement), the inelastic cross section is given by the equation

$$\frac{d\sigma}{d\Omega}(\text{inelastic}) = \int_0^{T_2} \frac{d\sigma(\text{inelastic})}{d\Omega dT} dT = \frac{\int_0^{T_2} n(T) dT}{m n_0 \omega}. \quad (4)$$

For such an energy spectrum of inelastically scattered electrons, Eq. (1) may be written as

$$N(h) = \int_0^{T_2} R(h,T) n(T) dT. \quad (5)$$

In the present measurements, the inelastic electrons in the above energy region produce the pulse-height distributions shown below the elastic peaks in Figs. 1–6, except for the contribution of the elastic tail. The areas A under the inelastic distributions in these figures are obtained by making linear extrapolations into the low-energy detector-noise region and by subtracting the contribution due to the area under the tail of the direct-beam curve. The uncertainties in the experimental values of the areas introduced by this procedure are estimated to be less than 20%, provided there is no radical change in the shape of the true spectrum in the low-energy noise region. From Eq. (5) these areas A are given by the equation

$$A = \frac{1}{c} \int_0^{h_2} N(h) dh = \frac{1}{c\epsilon} \int_0^{T_2} n(T) dT, \quad (6)$$

where c is the same proportionality constant as in Eq. (3). Therefore, from Eqs. (2)–(4) and (6), the ratio A/A_{DB} of the measured areas is given by the equation

$$A/A_{DB} = \frac{d\sigma}{d\Omega}(\text{inelastic}) \Big/ \frac{d\sigma}{d\Omega}(\text{elastic}). \quad (7)$$

This cross-section ratio is shown as a function of the scattering angle in Fig. 7 for the different atomic numbers and incident electron energies. The elastic cross sections ($d\phi/d\Omega$) (elastic) corresponding to the experimental ratios in these curves were evaluated from the exact formulas[10,11] and from the experimental data, that are available for this energy and angular region. The results for the experimental inelastic cross sections are shown by the points in Figs. 8 and 9. The uncertainty in these experimental points including both systematic and statistical errors is estimated to be ±20%.

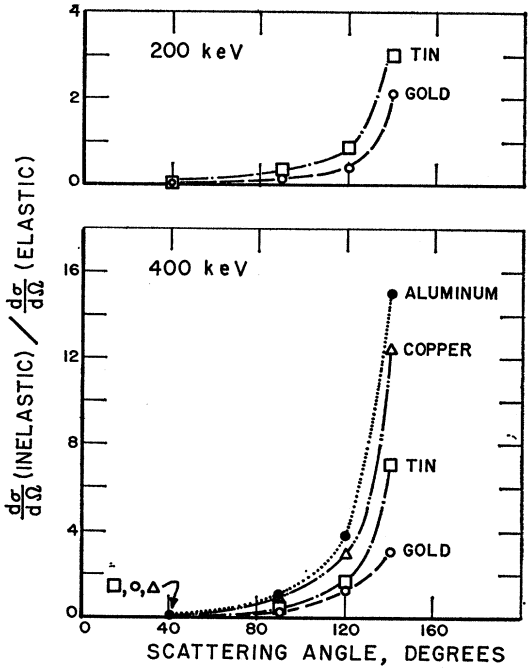

FIG. 7. Dependence of the cross-section ratio, inelastic to elastic on the electron scattering angle at incident-electron kinetic energies of 200 and 400 keV for aluminum (solid circles), copper (triangles), tin (squares), and gold (open circles) targets. The inelastic cross section is integrated over the scattered electron energies in the energy region involving large energy transfers below the elastic peak.

Figure 7 shows the following two features: (a) The ratio of the inelastic (as defined above) to the elastic cross sections becomes larger than unity for scattering angles larger than 90°, and (b) this ratio increases with decreasing atomic numbers at the specified incident electron energies of 200 and 400 keV. In the absence of exact calculations it is difficult to understand the behavior shown by feature (a). On the other hand feature (b) is consistent with the following qualitative argument. Inelastic scattering becomes proportional to the atomic number Z at large angles because of the decreasing importance of binding effects with large momentum transfers. Therefore, because elastic scattering is proportional to Z^2, the above cross section may be expected to decrease with Z for large scattering angles where the energy transfer is large compared to atomic binding energies.

The inelastic cross sections shown in Figs. 7–9 involve energy transfer which are large compared to the atomic binding energies. Therefore, as indicated in the previous

[9] J. W. Motz, R. C. Placious, and C. E. Dick, Phys. Rev. **132**, 2558 (1963).
[10] J. W. Motz, Haakon Olsen, and H. W. Koch, Rev. Mod. Phys. **36**, 881 (1964).
[11] Elmar Zeitler and Haakon Olsen, Phys. Rev. **162**, 1439 (1967); **136**, A1546 (1964); also Z. Naturforsch. **21a**, 1321 (1966).

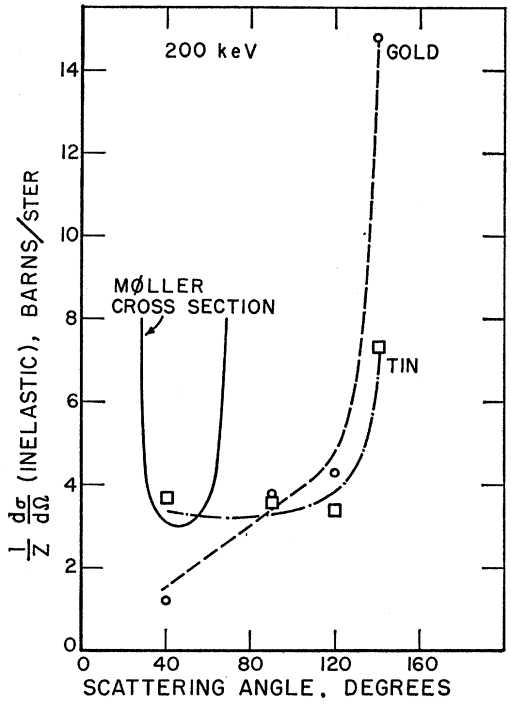

FIG. 8. Dependence of the experimental inelastic cross section per atomic electron per steradian, $(1/Z)(d\sigma/d\Omega)$, on the electron-scattering angle for 200-keV electrons incident on tin (squares) and gold (circles) targets. The theoretical Møller (Ref. 8) cross section for electron-electron scattering is indicated by the solid line.

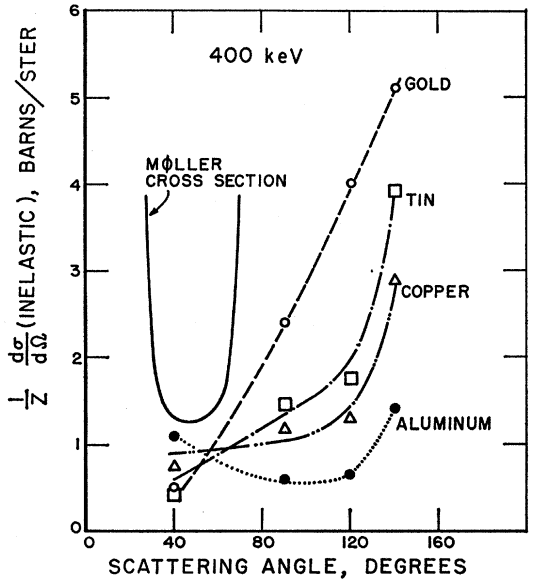

FIG. 9. Dependence of the experimental inelastic cross section per atomic electron per steradian, $(1/Z)(d\sigma/d\Omega)$, on the electron scattering angle for 400-keV electrons incident on aluminum (solid circles), copper (triangles), tin (squares), and gold (open circles) targets. The theoretical Møller (Ref. 8) cross section for electron-electron scattering is indicated by the solid line.

discussion, these cross sections most probably involve atomic ionization effects with the emission of an atomic electron. The small-angle nonrelativistic calculations of Morse[5] apply primarily to atomic excitation processes with small energy losses and cannot give a valid comparison with the present experimental results for ionization processes with large energy losses at large angles. The large-angle cross-section formula of Weber, Deck, and Mullin[6] is not applicable to the present measurements because it applied only to K-ionization events produced by extremely relativistic incident electrons, and in addition, it cannot be integrated over the energy of the scattered electron. In the absence of appropriate calculations which can be used to evaluate the inelastic ionization cross section, differential only with respect to the electron scattering angle, it is informative to show the behavior of the theoretical cross section predicted by Møller[8] for electron-electron scattering in which atomic binding effects are negligible. In Figs. 8 and 9, these theoretical Møller cross sections are compared with the experimental inelastic cross sections which are divided by the atomic number Z, $[(1/Z)(d\sigma/d\Omega)$ (inelastic)], in order to show how atomic binding effects influence the behavior of electron-electron scattering. These results show that because of the atomic binding effects, the Møller cross section does not accurately predict inelastic scattering processes for scattering angles in the region of 90°, and that there is an appreciable contribution to inelastic scattering for angles larger than 90°. This large-angle inelastic scattering increases sharply for scattering angles larger than 120°. In addition, the large-angle inelastic cross section increases both with the atomic number of the target and with the average binding energy per target electron. This behavior in which the inelastic cross section increases with the scattering angle above 120° cannot be predicted by any simple classical model involving binary collisions with a moving atomic electron. It is possible that double processes involving elastic and inelastic scattering in the same atom may be necessary to explain the effect. In any case, the experimental results indicate a need for exact, relativistic calculations of large-angle inelastic electron scattering processes, which are valid for incident-electron kinetic energies in the region of the electron rest energy.

ACKNOWLEDGMENT

The authors wish to thank Dr. Hans Kolbenstvedt for helpful discussions on inelastic scattering calculations.